Perturbed Equilibria of Myosin Binding in Airway Smooth Muscle: Bond-Length Distributions, Mechanics, and ATP Metabolism

Srboljub M. Mijailovich, James P. Butler, and Jeffrey J. Fredberg
Harvard School of Public Health, Boston, Massachusetts 02115 USA

ABSTRACT We carried out a detailed mathematical analysis of the effects of length fluctuations on the dynamically evolving cross-bridge distributions, simulating those that occur in airway smooth muscle during breathing. We used the latch regulation scheme of Hai and Murphy (*Am. J. Physiol. Cell Physiol.* 255:C86–C94, 1988) integrated with Huxley's sliding filament theory of muscle contraction. This analysis showed that imposed length fluctuations decrease the mean number of attached bridges, depress muscle force and stiffness, and increase force-length hysteresis. At frequencies >0.1 Hz, the bond-length distribution of slowly cycling latch bridges changed little over the stretch cycle and contributed almost elastically to muscle force, but the rapidly cycling cross-bridge distribution changed substantially and dominated the hysteresis. By contrast, at frequencies <0.033 Hz this behavior was reversed: the rapid cycling cross-bridge distribution changed little, effectively functioning as a constant force generator, while the latch bridge bond distribution changed substantially and dominated the stiffness and hysteresis. The analysis showed the dissociation of force/length hysteresis and cross-bridge cycling rates when strain amplitude exceeds 3%; that is, there is only a weak coupling between net external mechanical work and the ATP consumption required for cycling cross-bridges during the oscillatory steady state. Although these results are specific to airway smooth muscle, the approach generalizes to other smooth muscles subjected to cyclic length fluctuations.

INTRODUCTION

Load fluctuations are imposed continuously on airway smooth muscle and pulmonary vascular smooth muscle by the tidal action of breathing, and on muscular systemic arteries and arterioles by the pulsatile action of blood ejected from the heart. Smooth muscles in the urethra, urinary bladder, and gut are also subjected to periodic stretch. Imposed fluctuations in muscle load are a universal part of smooth muscle physiology.

It is well established that imposition of periodic load fluctuations on smooth muscle inhibits development of active force and stiffness (Warner and Gunst, 1992; Gunst et al., 1990; Fredberg et al., 1997). Although imposed load fluctuations induce important plastic changes in the cytoskeleton (Gunst et al., 1995; Pratusevich et al., 1995), a major part of the force and stiffness inhibitions that are observed are attributable to direct effects of tidal stretch upon bridge dynamics (Fredberg et al., 1997, 1999). With respect to activation, load fluctuations have little effect on subsequent post-vibration contraction, and it is unlikely that changes in load (stress) or length (strain) are responsible for modifying activation, although this is still unclear (Klemt et al., 1981; Peiper et al., 1996).

In a previous report we obtained insights into the contribution of bridge dynamics by analyzing the rigid sliding filament model of muscle contraction of Huxley modified to include latch regulation and the four myosin states described by Hai and Murphy (1988a, b) and Fredberg et al. (1999). The mathematical synthesis of the ideas of Huxley with those of Hai and Murphy we refer to as HHM theory (Fredberg et al., 1999). Here we report a further analysis of HHM theory and focus in particular on the myosin bond length distributions. We examined how these distributions are perturbed by periodic changes of muscle length and how these distributions lead to changes in muscle mechanics and in the rate of ATP utilization. These results may help to explain why airway narrowing is limited in healthy lungs, but can become excessive in asthmatic lungs.

Received for publication 17 March 2000 and in final form 3 August 2000.

Address reprint requests to Srboljub M. Mijailovich, Physiology Program, Department of Environmental Health, Bldg. I, Room 1304e, Harvard School of Public Health, 665 Huntington Avenue, Boston, MA 02115. Tel.: 617-432-3482; Fax: 617-432-4710; E-mail: smijailo@hsph.harvard.edu.

0006-3495/00/11/2667/15 $2.00

METHODS

Hai and Murphy (1988a) defined the four-state myosin model to comprise free unphosphorylated myosin (M), phosphorylated myosin (Mp), phosphorylated myosin attached to actin (AMp), and unphosphorylated myosin attached to actin (AM, also called latch bridges) (Fig. 1 *A*). As in their work, we assumed that both AMp and AM cross-bridges have the same stiffness, and that ATP binding is a prerequisite for detachment. The transitions among the four states are governed by seven rate constants (Fig. 1 *A*). Implicit in the scheme is that cross-bridges cannot attach to actin unless they are first phosphorylated, i.e., the muscle is regulated exclusively by Ca^{2+}-dependent state transition rate constants, k_1 and k_6 (which may vary with time), mediated by calmodulin-dependent myosin light chain kinase (MLCK). Hai and Murphy also assumed that the affinities of MLCK and myosin light chain phosphatase (MLCP) for both attached and detached cross-bridges are similar, i.e., $k_1 \approx k_6$ and $k_2 \approx k_5$.

We assessed the relationship among the time-varying external load, level of muscle activation, and actomyosin dynamics by computing numerical solutions to the HHM theory. This theory can be written as four coupled partial differential equations that express conservation of each myosin species, which in vector form becomes,

$$D\mathbf{n}(x, t)/Dt = \mathbf{T}(x, t)\mathbf{n}(x, t). \quad (1)$$

Each of the four components of the vector $\mathbf{n}(x, t)$ corresponds to the population fraction of myosin in one of its four states (i.e., $n_M(x, t)$, $n_{M_p}(x,$

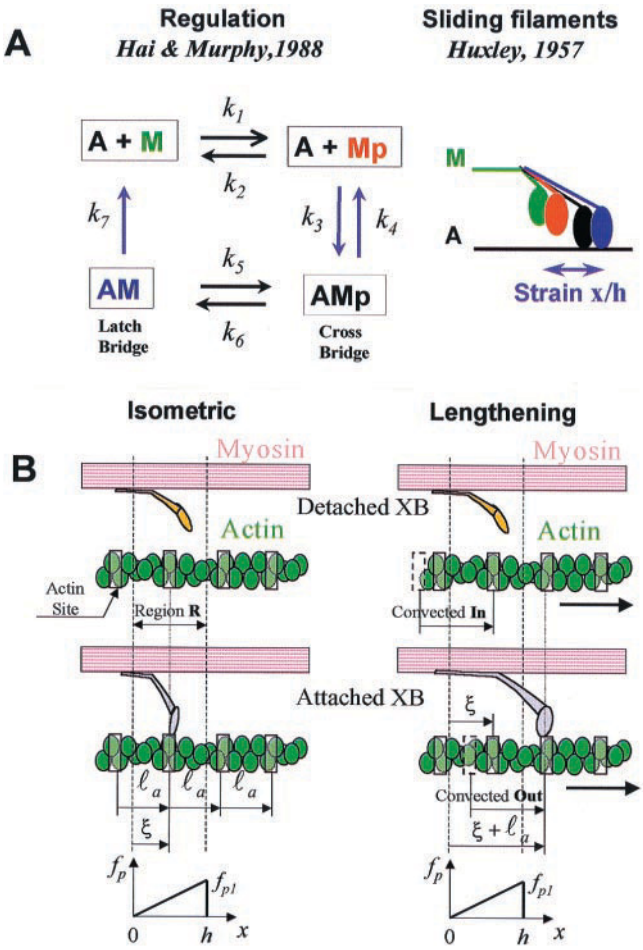

FIGURE 1 (*A*) Hai and Murphy's four-state model: the latch regulatory scheme for Ca^{2+}-dependent smooth muscle activation and Huxley's sliding filament model. A actin (thin filament); myosin cross-bridge states are M (detached, unphosphorylated); Mp (detached, phosphorylated); AMp (attached, phosphorylated); AM (attached, unphosphorylated, also known as the latch bridge). k_1–k_7 are first-order rate constants from experimental data (Hai and Murphy, 1988a). k_1 and k_6 represent Ca^{2+}, calmodulin-dependent myosin light chain kinase (MLCK) activity; k_2 and k_5 represent myosin light chain phosphatase (MLCP) activity, where k_5 drives the rapidly cycling cross-bridges, AMp, to slowly cycling latch bridges, AM. k_3 and k_4 are the rate constants for attachment and detachment of phosphorylated cross-bridges, and k_7 is the rate for latch bridge detachment, all three dependent on cross-bridge displacements (x) through scaled Huxley's attachment and detachment (spatially distributed) rates. h: range of displacements over which myosin has a positive binding rate. (*B*) Conservation of the number of cross-bridges: the attachment region R is defined to be the interval $0 < x < h$, where f_p is positive; ξ is a local coordinate of the actin site available in R; ℓ_a is the distance between actin sites (shown as semi-transparent *solid line boxes*). *Left*: Isometric case—an available myosin head corresponds to a detached cross-bridge. *Right*: After lengthening, some myosin heads are drawn away (convected out) from the attachment region while still attached (*right lower panel*), and at the same time some unoccupied actin sites are moved within R (convected in). Semi-transparent dashed line boxes represent some actin sites before lengthening, while solid line boxes represent actin sites after lengthening.

t), $n_{AM_p}(x, t)$, $n_{AM}(x, t)$), all of which vary both in time, t, and space, x, where x is the position of the active actin site on the actin filament relative to the equilibrium position of the cross-bridge on the myosin filament (Huxley, 1957). The operator D/Dt is the material derivative $\partial/\partial t - V(t)\partial/\partial x$, also called the convective derivative, where $V(t)$ is the velocity of the actin filament relative to myosin filament and is traditionally taken to be positive during shortening. This derivative expresses the time rate of change in a coordinate system moving (convecting) with the myosin filament. It contains two distinct terms: first, the independent rate of change with time at fixed position x in the laboratory frame, and second, the rate of change associated with motion of the moving myosin filament where, due to the presence of spatial gradients, there is a difference in cross-bridge populations entering and leaving the differential element dx.

The 4×4 rate transition matrix $\mathbf{T}(x, t)$ describes the probability of transitions between these states, and how these probabilities vary with position of the myosin head. These probabilities are important because, with any relative movement between actin and myosin filaments, the myosin head may traverse regions that tend to favor attachment events, and some others that tend to favor detachment events; the latter dominate where x is large and or negative (Huxley, 1957). The elements of $\mathbf{T}(x, t)$ include both the position-*independent* transitions between M and Mp and between AM and AMp (phosphorylation and dephosphorylation of 20 kD myosin light chain are driven by action of kinases and phosphatases (Hai and Murphy, 1988a, b)), and position-*dependent* transitions between Mp and AMp and between M and AM (attachment and detachment of myosin to actin (Huxley, 1957; Hai and Murphy, 1988b)). As such, $\mathbf{T}(x, t)$ governs the transition of chemical events into mechanical events and, importantly, the converse as well. To set $\mathbf{T}(x, t)$, we used the rate functions reported by Hai and Murphy after adapting them to include the increased rate of detachment (g_3) described by Zahalak (1986) in the region $x > h$, where h is the range for positive probability of attachment (Huxley, 1957). The rate transition matrix is:

$$\mathbf{T}(x, t) = \begin{bmatrix} -k_1(t) & k_2 & 0 & g(x) \\ k_1(t) & -k_2 - f_p(x) & g_p(x) & 0 \\ 0 & f_p(x) & -k_5 - g_p(x) & k_6(t) \\ 0 & 0 & k_5 & -k_6(t) - g(x) \end{bmatrix} \tag{2}$$

where

$$f_p(x) = \begin{cases} 0, & x < 0 \\ f_{p1}x/h, & 0 \le x \le h \\ 0, & h < x \end{cases}$$

$$g_p(x) = \begin{cases} g_{p2}, & x < 0 \\ g_{p1}x/h, & 0 \le x \le h \\ (g_{p1} + g_{p3})x/h, & h < x \end{cases}$$

$$g(x) = \begin{cases} g_2, & x < 0 \\ g_1x/h, & 0 \le x \le h \\ (g_1 + g_3)x/h, & h < x. \end{cases} \tag{3}$$

$f_p(x)$ is the position-dependent attachment rate of Mp, $g_p(x)$ is detachment rate of AMp, and $g(x)$ is the detachment rate of AM. The subscript p denotes phosphorylated myosin heads. Following Hai and Murphy (1988a,b), the attachment rate of unphosphorylated myosin (i.e., M → AM) is negligible, which accounts for that 0 entry in $\mathbf{T}$. Note also that the Ca^{2+}-dependent transition rates k_1 and k_6 to the phosphorylated states are explicitly shown as potential functions of time. The magnitude of the above

rate-dependent cross-bridge constants, defined by f_{p1}, g_{p1}, and g_1, are chosen to match Murphy's position-independent state transition rate constants, k_3, k_4, and k_7, respectively, when relations (3) are averaged over x. Specifically, the linear character of the rate constants within $0 \le x \le h$ implies, for example, that the average of $f_p(x)$ is simply $f_{p1}/2$. Thus we take $f_{p1} = 2k_3$; g_{p1} and g_1 are evaluated similarly. Finally, we evaluated the other time constants to be $g_{p2} = 4(f_{p1} + g_{p1})$ and $g_2 = 20\, g_1$ as defined in Huxley (1957), and $g_{p3} = 3g_{p1}$ and $g_3 = 3g_1$ as defined in Zahalak (1986).

Conservation of the number of cross-bridges (myosin heads)

Huxley (1957) assumed that for every unoccupied actin site there is always an available myosin head, and also that only one myosin head per cross-bridge can attach at any instant of time. Thus, an available myosin head corresponds to a detached cross-bridge. This is correct for the isometric case, but when shortening or lengthening is allowed, some myosin heads are drawn away from the attachment region R (defined to be the interval $0 < x < h$, where f_p is positive) while still attached, and at the same time some unoccupied actin sites are moved within R (Fig. 1 *B*). In order to satisfy Huxley's original assumption, the attached myosin head that was convected outside R (i.e., physically moved outside that region), cannot attach to the actin site within R until that myosin head detaches. To correct for this, following the work of Piazzesi and Lombardi (1995), we specify that a myosin cross-bridge, which repeats along the filament axis with a periodicity of ℓ_m, can attach only to one actin site within R. We define ξ as a local coordinate of the actin site available in R (thus $0 < \xi < h$). We also assume that after detachment a cross-bridge rapidly (of order of tens of microseconds) regains its original configuration, thus the myosin head can reattach to one actin site in R, and therefore all detached states $n_M(\xi, t)$ and $n_{M_p}(\xi, t)$) are also only in R. This condition ensures that the total number of myosin species is conserved. During lengthening or shortening, the attached myosin heads convect out of R, decreasing the number of actin sites available for the attachment in R. Thus, the requirement that the sum of the probabilities over all possible states translates, for all ξ, to the condition:

$$n_{Mp}(\xi, t) + n_M(\xi, t) + \sum_m [n_{AMp}(\xi + m\ell_a, t) + n_{AM}(\xi + m\ell_a, t)] = 1,$$

where ℓ_a is the distance between actin sites (conveniently assumed to be equal to h), and m indexes the actin lattice, with spatial period ℓ_a.

Numerical solution

The vector $\mathbf{n}(x, t)$ is obtained by solving Eq. 1 numerically using the method of characteristics described earlier (Mijailovich et al., 1996). Specifically, integrations were performed with 1000 time steps per cycle and with 800 length steps per h. The instantaneous force was computed from the first spatial moment of the attached cross-bridge state number distribution $n_{AM_p}(x, t) + n_{AM}(x, t)$, integrated over all x. Similarly, the instantaneous state population fractions, denoted M(t), Mp(t), AMp(t), and AM(t), were computed from the zeroth spatial moment of the number state distributions. In steady state, ⟨M⟩, ⟨Mp⟩, ⟨AMp⟩, and ⟨M⟩ denote the respective average values over one period. During isometric force development instantaneous force is explicitly computed from $\mathbf{n}(x, t)$.

The rate of ATP consumption was separately computed for each of the four transition processes indicated in Fig. 1:

the detachment of Mp from AMp:

$$\int_{-\infty}^{\infty} g_p(x) n_{AM_p}(x, t)dx/h,$$

the detachment of M from AM:

$$\int_{-\infty}^{\infty} g(x) n_{AM}(x, t)dx/h,$$

the phosphorylation of M:

$$k_1(t) \int_{-\infty}^{\infty} n_M(x, t)dx/h,$$

and the phosphorylation of AM:

$$k_6(t) \int_{-\infty}^{\infty} n_{AM}(x, t)dx/h.$$

The total ATP consumption rate (denoted ATP_{tot} in the figures) is the sum of these four terms. The cyclic rate of ATP consumption (denoted ATP_{cycl} in the figures) is designated as that component associated only with bridge detachments, i.e., the sum of the first two terms above. In particular, in steady state, the average (over one period) cross-bridge cycling rate is proportional to the average ATP_{cycl}. Average fractional phosphorylation of myosin was calculated as ⟨Mp⟩ + ⟨AMp⟩. Similarly, the average myosin duty cycle is given by ⟨AMp⟩ + ⟨AM⟩.

Initial conditions

We assumed that all cross-bridges were in the detached unphosphorylated state in relaxed tissue, i.e., $n_M(x, 0) = 1$, $x \in R$; the other population fractions being zero. Initially we take $k_1 = k_6 = 0$, corresponding to a $[Ca^{2+}]$ below the threshold for MLCK activation (Hai and Murphy, 1988a).

Loading conditions, time averaging, and dynamic moduli

We considered isometric force development at optimal length, L_0, and sinusoidal length variations about the optimal length, $L(t) = L_0 + \Delta L \sin 2\pi ft$, where ΔL is the stretch amplitude and f is frequency. Muscle activation is taken into account by setting the phosphorylation rate constants $k_1(t)$ and $k_6(t)$ to mimic the initial Ca^{2+} transient during force development (Hai and Murphy, 1988a). The mean values of force, stiffness, and ATP consumption were calculated by time-averaging their instantaneous values over the tidal stretch cycle. From closed force-length loops (see Note 1 at end of text) the values of muscle elastance, E, and hysteresivity, η, were computed on a loop-by-loop basis in the following manner. If D is energy dissipated through external work per period of imposed cyclic stretch (i.e., area within the force-length loop) and ΔF is the amplitude of phasic force variation about F, then we use the following relations, which remain useful even when the loop becomes non-elliptical, which is indicative of nonlinear mechanical behavior (Fredberg and Stamenovic, 1989; Fredberg et al., 1996, 1997), $E = (\Delta F/\Delta L) \cos \phi$, and $\eta = \tan \phi$, where $\phi = \sin^{-1}(D/\pi \Delta F \Delta L)$. Force (instantaneous and mean), stiffness (instantaneous and mean), and E (only defined over a cycle) were normalized to the force,

stiffness, and stiffness, respectively, under fully developed isometric conditions at 100% phosphorylation.

The numerical parameter values used in simulations were as follows. The state transition constants for airway smooth muscle, adapted from Hai and Murphy (1988a), were $k_1(t) = k_6(t) = (0.35s^{-1}, 0 < t < 5$ s; and 0.060 s^{-1}, 5 s $< t$), $k_2 = k_5 = 0.1\ s^{-1}$, $k_3 = 0.44\ s^{-1}$, $k_4 = k_3/4 = 0.11\ s^{-1}$, $k_7 = 0.005\ s^{-1}$. The attachment and detachment rate constants of the Huxley scheme f_{p1}, g_{p1}, and g_1, are taken to be twice k_3, k_5, and k_7, respectively, in order to approximately preserve the average values of the latter during force development (see Note 2), namely $f_{p1} = 0.88\ s^{-1}$, $g_{p1} = 0.22\ s^{-1}$, $g_1 = 0.01\ s^{-1}$. The other constants, related to $x < 0$, are $g_{p2} = 4(f_{p1} + g_{p1}) = 4.40\ s^{-1}$ and $g_2 = 20g_{p1} = 0.20\ s^{-1}$ (this proportion is originally defined by Huxley, 1957, and slightly adjusted by Hai and Murphy, 1988 b), and related to $x > h$ are $g_{p3} = 3g_{p1} = 0.66\ s^{-1}$ and $g_3 = 3g_3 = 0.03\ s^{-1}$ (Zahalak, 1986). The remaining parameters in the problem were taken to be 1) crossbridge strain is 36% of overall strain to account for the serial elastic component (Mijailovich et al., 1996); 2) the myosin distortion displacement scale (h) is 15.6 nm (Huxley, 1957); and 3) the sarcomere length is 2.2 μm (Hai and Murphy, 1988b). For scaling purposes, note that a crossbridge displacement of magnitude h corresponds to a whole muscle strain of $\sim\varepsilon = \Delta L/L_0 = 4\%$.

RESULTS AND DISCUSSION

Bond length distributions during isometric force development

Fig. 2 shows the evolution of the bond distributions of the attached myosin populations, AMp and AM, during isometric force development. Before activation all myosin molecules are found in the unphosphorylated unattached pool (M); this pool becomes rapidly depleted with stimulus onset, however, as myosin molecules become phosphorylated and then attach to the actin filament forming the species AMp. During this early period of isometric force develop-

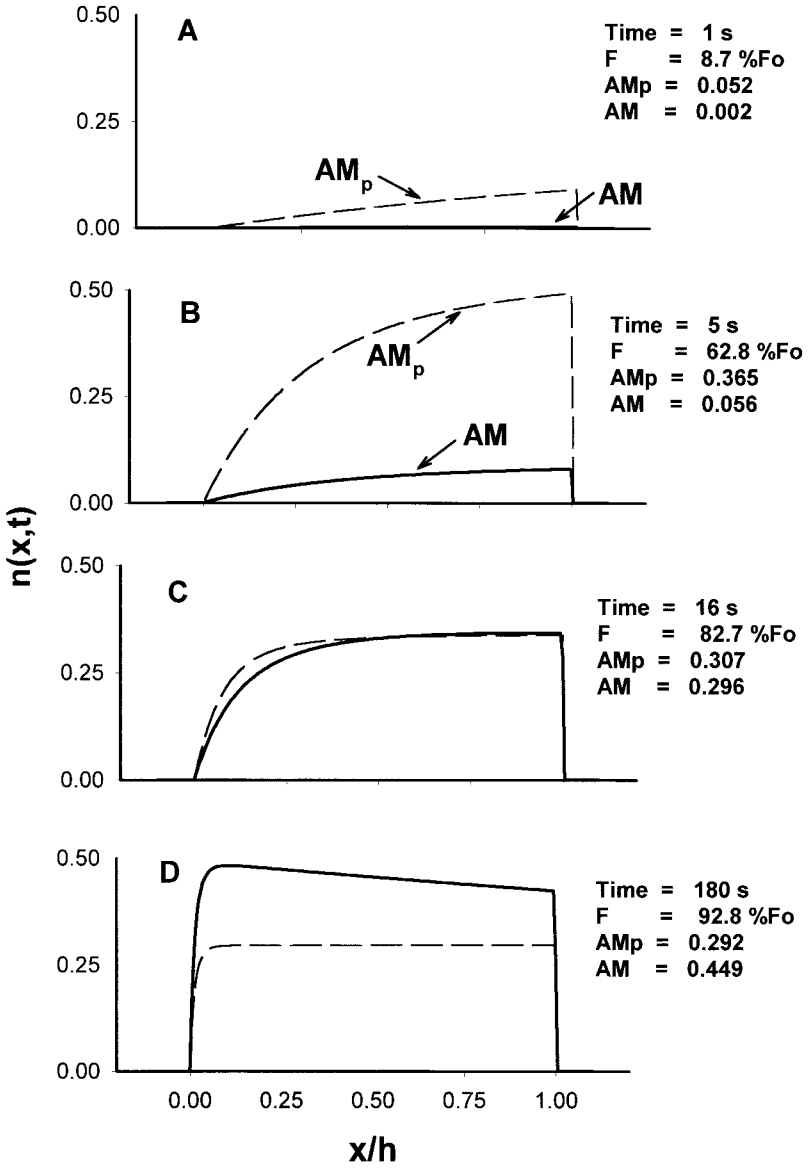

FIGURE 2 The evolution of the bond distributions during isometric force development of the phosphorylated and unphosphorylated attached myosin populations, AMp (*dashed line*), and AM (*solid line*) at four distinctive times; during the early Ca^{2+} transient (1 and 5 s, panels *A* and *B*), and at later times during force development, characteristic of the formation of the "latch state" (16 and 180 s, panels *C* and *D*).

ment, the spatial distribution of $n_{AM_p}(x, t)$ is roughly linear in x, and corresponds closely to the linear spatial dependence of the attachment rate function in the region $0 < x < h$ (Fig. 2 *A*). As time passes, $n_{AM_p}(x, t)$ becomes more spatially uniform, however, as attachment and detachment events approach a rough balance (Fig. 2, *B–D*). This balance is first achieved at positions close to $x = h$, where $f_p(x)$ and $g_p(x)$ are the largest (see *dashed line* in Fig. 2 *B*). As time passes, this equilibration process propagates toward smaller x, where rate constants are slower (Fig. 2 *C*). In the steady state, $n_{AM_p}(x, t)$ approaches a limit that is approximately (but not exactly) constant with x (Fig. 2 *D*).

The AM pool is the last to be populated, because it can grow only from the developing AMp pool. At short times ($t < 1$ s) $n_{AM}(x, t)$ is small compared to $n_{AM_p}(x, t)$, then gradually increases. From the onset of contraction up to ~16 s, the $n_{AM}(x, t)$ is $< n_{AM_p}(x, t)$, but has a roughly similar shape due to the fact that the AMp → AM transition is independent of x. The two distributions are approximately equal at ~16 s (Fig. 2 *C*). At later stages of force development, the distributions approach their respective steady states (Fig. 2 *D*), and the population of the AM pool exceeds that of the AMp for all x.

The bond length distributions of AMp and AM in the isometric steady state (Fig. 2 *D*) correspond to a static equilibrium of myosin binding and is what Hai and Murphy called the "latch state." In this isometric steady state the distribution of $n_{AM}(x, t)$ is clearly nonuniform. The reason for this nonuniformity can be understood by considering a mass balance of the AM species. Flux of molecules into the AM pool arises from dephosphorylation of AMp, but that transition rate is independent of position x. The net flux of molecules out of the AM pool, however, arises from a detachment process (the AM → M pathway) that favors a greater rate of detachment at greater values of x. In the steady state these fluxes must be balanced and, as a result, $n_{AM}(x, t)$ is spatially nonuniform.

Fig. 3 *A* shows the rapid increase in phosphorylation during the early Ca^{2+} transient (0–5 s), followed by a rapid increase in force F and instantaneous stiffness K. The increase in F and K correspond to the increasing number of both AM and AMp bridges. Both F and K continue to increase during the subsequent decrease in phosphorylation, but at a much slower rate. From roughly 5–16 s, this slow increase in F and K is associated with transitions of bridges from the AMp pool to the AM pool (compare the second and third panels of Fig. 2). The final relative populations of the AMp and AM states depend upon the level of fractional phosphorylation. In the example shown the steady-state fractional phosphorylation is 0.375, for which the population of AM bonds ultimately exceeds the AMp population. This partitioning is typical for low levels of fractional phosphorylation and corresponds to the "latch state" (Hai and Murphy, 1988a).

Imposition of length fluctuations

As shown in Fig. 3, *A–C*, we imposed sinusoidal changes in muscle length ($\Delta L = 1\%$ of L_0) at $t = 180$ s, followed by a change in amplitude to 4% of L_0 at $t = 245$ s. These oscillatory perturbations in muscle length upset the isometric binding equilibrium and cause it to adapt to a new perturbed equilibrium of myosin binding. The dynamic steady state is characterized by fewer attached bridges, lower mean force, lower stiffness, and higher mean ATP consumption, even though the level of phosphorylation remains unchanged. These effects are caused by increased detachment of cross-bridges exposed to high detachment rates when convected out of the attachment region ($0 < x < h$). It is interesting to notice that the instantaneous force, F, and ATP_{cycl} substantially vary over the cycle, while the instantaneous stiffness, K, and populations of AM and AMp species vary only modestly (Fig. 3, *A–C*, $t > 180$ s). This behavior is fully determined by the underlying cyclic changes in the cross-bridge bond distributions $\mathbf{n}(x, t)$, to which we now turn.

Perturbed equilibria of myosin binding

Fig. 4 shows the underlying AMp and AM bond distributions as a function of x at two amplitudes and two frequencies. When subjected to very small tidal stretches ($\Delta L/h < 0.5$ or $\varepsilon < 2\%$), as shown in the left column of Fig. 4, the middle portion of the steady-state $n_{AM}(x, t)$ and $n_{AM_p}(x, t)$ bond distributions remains virtually the same as in the steady isometric condition. This is because the cross-bridges there never leave the region $0 < x < h$, where the ratio $f_p/(f_p + g_p)$ is constant, and the effect of the much slower detachment rate g (AM → M) is small. However, the left and right shoulders of $n_{AM}(x, t)$ and $n_{AM_p}(x, t)$ sample the regions $x < 0$ and $x > h$ for some fraction of the cycle, and they are modified accordingly. The number of cross-bridges in the shoulders decreases with increase of amplitude of tidal stretch and/or increase of time that these populations of cross-bridges spend during sampling these high detachment rate regions.

For larger tidal stretches ($x/h > 0.5$ or $\varepsilon > 2\%$), as shown in middle column of Fig. 4, all cross-bridges sample the regions $x < 0$ and $x > h$, where no attachment events occur and overall detachment rate functions (in particular g_p, driving the AMp → Mp transition) are high. This causes a redistribution of $n_{AM}(x, t)$ and $n_{AM_p}(x, t)$, with a general depression in their overall levels, compared with the isometric steady state. This reduction in the number of attached bridges, taken together with the alterations of their distributions, are consistent with the inhibition of force and stiffness caused by imposed tidal changes in muscle length shown in Fig. 3 *A*. Indeed, at larger amplitudes (>4%), not only the number of bridges is smaller, but also AMp(t) is greater than AM(t) in contrast to both the isometric and low

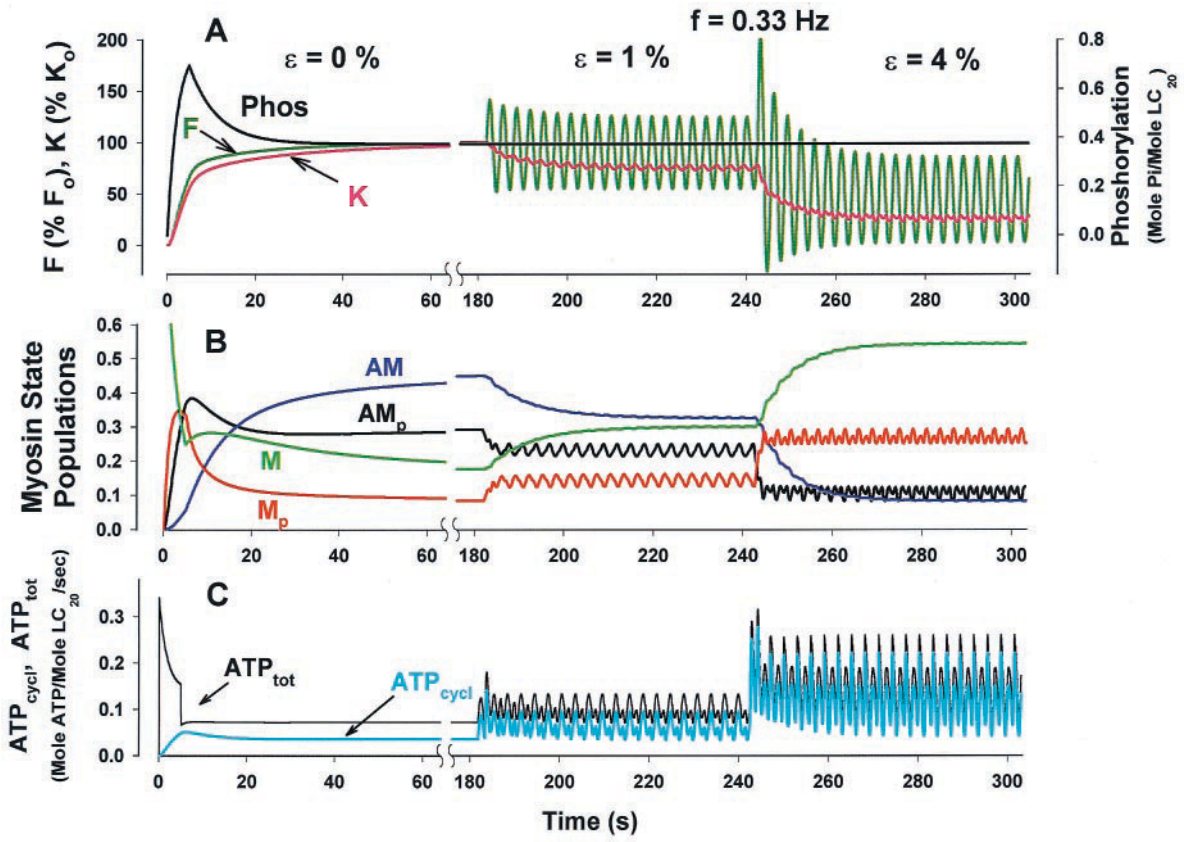

FIGURE 3 Evolution of mechanical and metabolic parameters during force development (0–180 s) and superimposed length variations of 1% (180–245 s) and 4% (245–305 s). (*A*) During force development, phosphorylation (*black*) peaks at ~5 s, following the Ca^{2+} transient (through k_1 and k_6), while muscle force, *F* (*dark green*), and instantaneous stiffness, *K* (*pink*), monotonically increase, more slowly than phosphorylation, and they stay at high levels. Superimposed length variations of 1% and 4% did not affect levels of myosin phosphorylation, but progressively depressed both mean *F* and mean *K*, but while instantaneous *F* fluctuated >50% of its isometric value, instantaneous *K* only modestly varied over its mean value. (*B*) State population transitions of M (*green*), Mp (*red*), and AMp (*black*) occurred quickly and the muscle force and stiffness developed mostly through rapid cross-bridge cycling. Latch bridges (AM, *blue*) developed later (from 5 to 15 s), significantly slowing the apparent cross-bridge cycling rates, and their contribution to the developed force and stiffness gradually increased. Imposed strain variations decreased the numbers of both AMp and AM bridges, but the decrease of AMp was more prominent at higher strains. Variation of all state populations was small compared to *F*, and almost unnoticeable for unphosphorylated M and AM species. (*C*) Total ATP consumption (*black line*) first dropped, reflecting the early transient between M and Mp states, then increased following initial increase of cross-bridge cycling rates (i.e., ATP_{cycl}, *cyan line*), and reached a plateau at larger times (~180 s). Imposed length variations increased cycling rates and ATP_{cycl} of both AMp and AM bridges.

amplitude cases, where the AM(t) population systematically exceeds the AMp(t) population (Fig. 3 *B*, $t < 245$ s, Fig. 4, *left column*).

This reversal of the AMp(t)/AM(t) ratio at larger length fluctuations is caused by an increased overall rate of detachment events for AMp and AM, and increased attachment events for Mp compared with isometric steady conditions or the small amplitude length variations. This is consistent with higher average cycling rates of attachment and detachment transitions, and with tidal stretch augmentation of both hysteresivity and the rate of ATP_{cycl} utilization, as shown in Fig. 3 *C*.

When the frequency of sinusoidal length variations is small compared to the smallest typical rate constant (here given by g_1h, the typical detachment rate for the latch bridges), both bond distributions, $n_{AM}(x, t)$ and $n_{AM_p}(x, t)$, approach the steady-state distribution similar to the steady-state shortening or lengthening velocity profiles. In that circumstance the cyclic behavior approximates a sequence of quasi-steady dynamic states for shortening or lengthening (not shown). When the frequency is of order g_2 (the next smallest rate), but still small compared to the rate constants of rapid cycling cross bridges, only $n_{AM_p}(x, t)$ exhibits the quasi-steady-state distribution associated with the instantaneous muscle velocity, while $n_{AM}(x, t)$ significantly varies both in space and time. This is shown in Fig. 4, right column, where $n_{AM_p}(x, t)$ approximates the steady "box" shape for all times except near $t = 0$; the time of maximum positive velocity. By contrast, $n_{AM}(x, t)$ displays a very complex shape throughout the cycle. At higher frequencies

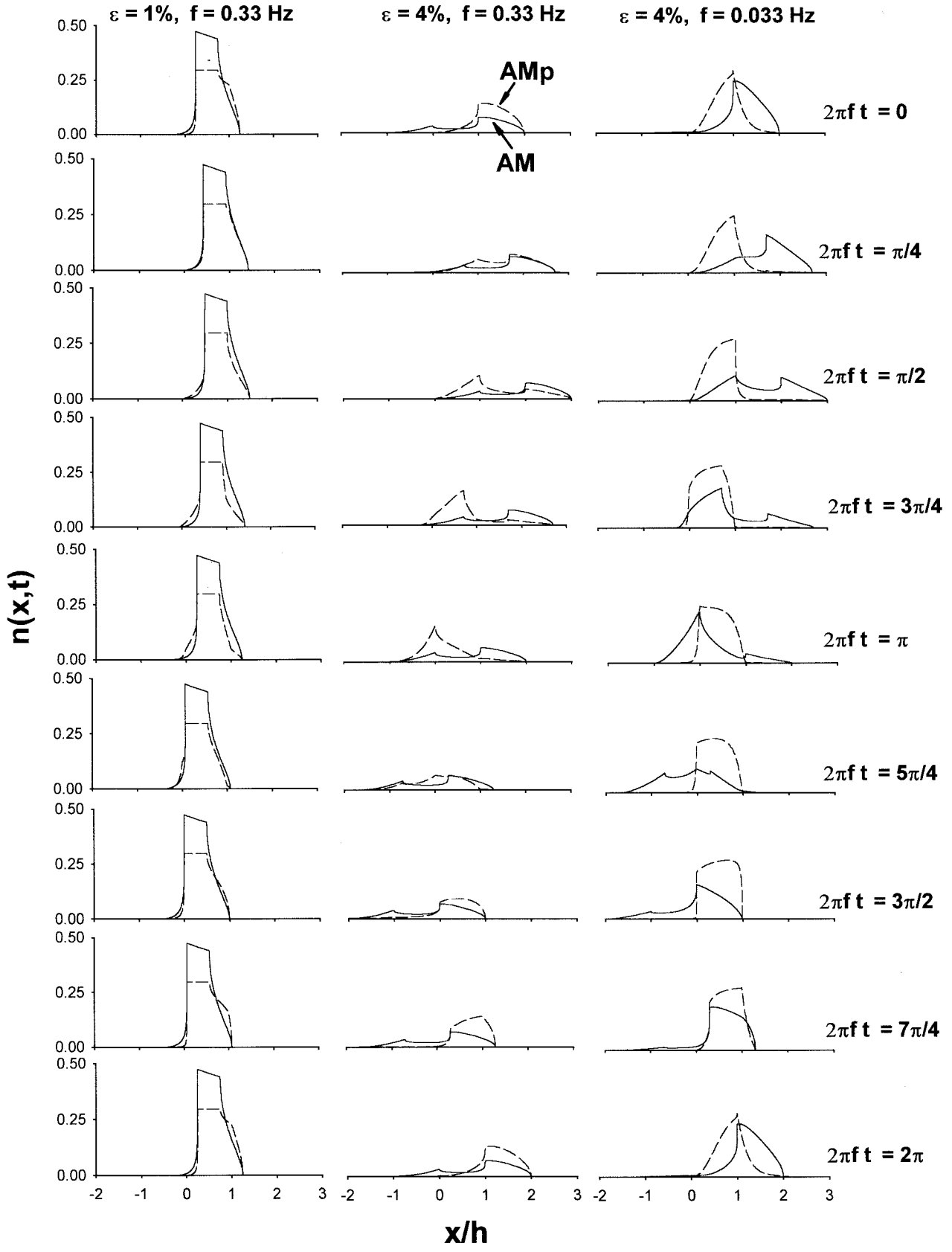

FIGURE 4 The bond distributions of attached myosin populations AMp (*dashed line*), and AM (*solid line*) at eight distinctive times during a steady-state cycle for three combinations of 1% and 4% stretch amplitudes, and 0.33 and 0.033 Hz frequencies.

(larger than g_2), $n_{AM}(x, t)$ convects back and forth during each cycle with a shape that is almost time-invariant, while $n_{AM_p}(x, t)$ varies in space and time (not shown). At very high frequencies (much larger than g_{p2}), however, both $n_{AM}(x, t)$ and $n_{AM_p}(x, t)$ have shapes that are approximately time-invariant (not shown) and the muscle behaves as a purely elastic system.

Dynamically determined contractile states

Force-length loops

The instantaneous force generated by either rapidly cycling or latch bridges is proportional to the first moments of $n_{AM_p}(x, t)$ and $n_{AM}(x, t)$, respectively. The total force is the sum of the forces from these two populations. As remarked above, at high frequencies the bond distribution shapes of both attached species are approximately time-invariant and simply shift back and forth during oscillation. The first moments of these convecting distributions are therefore proportional to the displacement, and thus all forces (partial and total) vary nearly linearly with length. At moderate frequencies and small amplitudes the latch bridge distribution, but not the rapidly cycling distribution, continues to approximate a more or less fixed shape which, by the argument above, contributes a force that is linear in displacement. By contrast, the rapidly cycling cross-bridge distribution changes substantially over time and displays a correspondingly hysteretic force/length characteristic. These two phenomena are shown in the upper left panel of Fig. 5.

The physiological range of tidal stretches for airway smooth muscle at the actin and myosin filament level is on the order of h (i.e., $\varepsilon = \Delta L/L_0 = 4\%$) (see Note 3) and the range of frequencies is comparable to the detachment rates (e.g., the detachment rate constant $g_{p1} = 0.22\ s^{-1}$ is comparable to quiet breathing frequency in humans of 0.2 Hz, or dogs of 0.30 Hz (Altman and Dittmer, 1974). The shapes of $n_{AM}(x, t)$ and $n_{AM_p}(x, t)$ therefore approximate neither the high nor low frequency limits (respectively a purely elastic system or a constant force generator). As shown in Fig. 5, middle and right panels, this results in clockwise force-length loops that systematically fall below the static operating point (i.e., 100% F_0). With respect to force, therefore, the muscle state is dynamically determined. Similarly, just as the forces arise from the first moment of the distribution functions, the instantaneous stiffness is given by the zeroth moment. In the physiologic range of amplitudes and frequencies, these moments also fail to approximate either the high or low frequency limits (both of which display constant stiffness over the cycle). The bottom portion of Fig. 5 shows

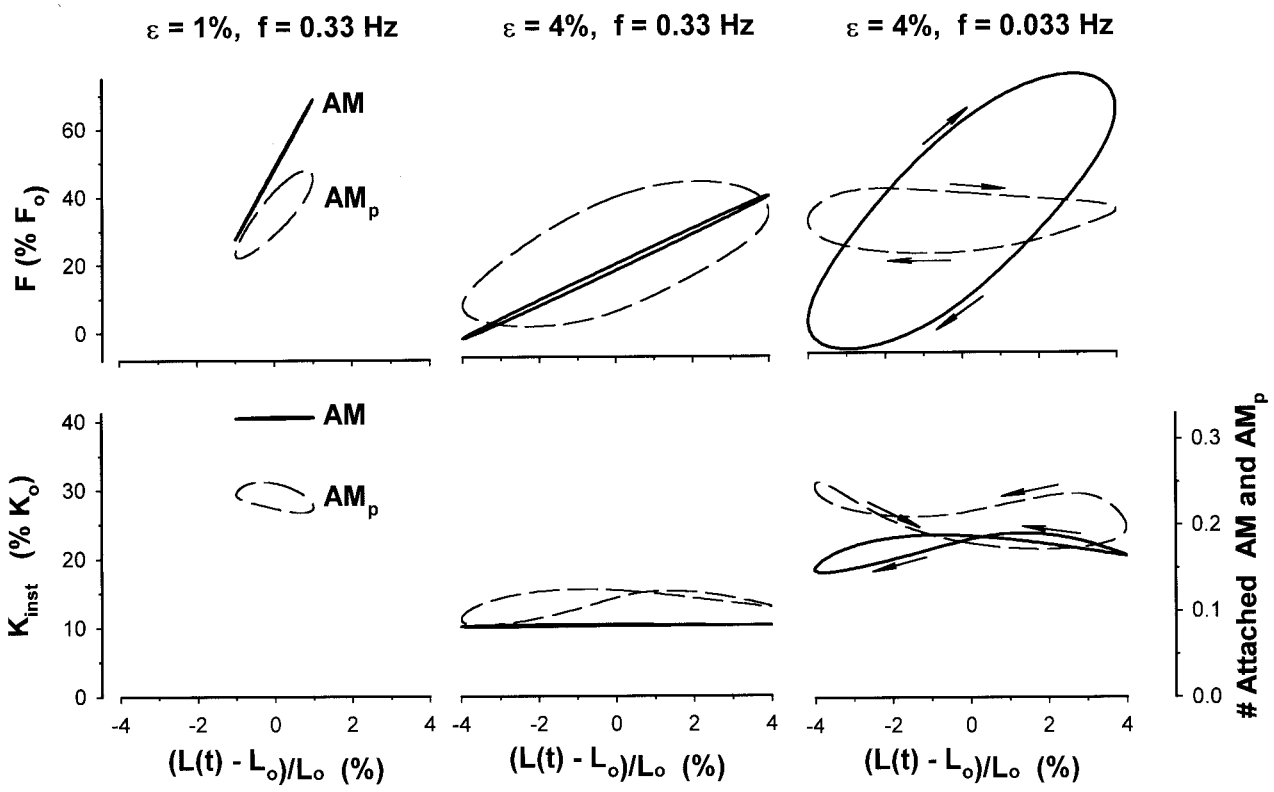

FIGURE 5 Force–length loops and instantaneous stiffness–length loops of the partial contributions of $n_{AM_p}(x, t)$ (*dashed line*) and $n_{AM}(x, t)$ (*solid line*) for the same combinations of amplitudes and frequencies as in Fig. 4. Instantaneous force and stiffness are normalized to their isometric values.

these cyclic variations in instantaneous stiffness, separated into the contributions from AM and AMp populations. Thus, it follows that with respect to stiffness as well, the muscle state is now dynamically determined.

The total force and the total stiffness loops as a function of strain amplitude for a frequency of 0.33 Hz (similar to spontaneous breathing) are shown in Fig. 6 (*left panels*). In this case, increasing tidal stretch amplitude systematically decreased the mean total force and the slopes of the loops, but increased the loop "fatness." The instantaneous stiffness dropped markedly with increasing stretch amplitude, but varied little over cycle. For smaller strain amplitudes (up to 2% of L_0), the force-strain loops are remarkably similar to the loops measured in fully activated bovine tracheal muscle set to a mean length of L_0 (compare to Fig. 1 in Fredberg et al., 1997). However, for larger strains the HHM model loops failed to predict banana-shaped loops. The origin of this discrepancy may lie in the lack of details in Huxley's detachment rate functions at larger stretches (Harry et al., 1990) and/or nonlinear serial elastic component (Seow and Stephens, 1987). The right panels show families of loops in physiological range of frequencies for (fixed) stretch amplitude of 4%. In this case, increasing frequency decreased mean force and loop "fatness," with little effect on loop slope. Increasing frequency also induced a sharp drop in instantaneous mean stiffness.

Fractional contributions of AMp and AM cross-bridges to mean force, stiffness, and hysteresivity: stretch amplitude and frequency-dependence

Fig. 7 shows the fractional contributions of AM and AMp bridges to mean force F, elastance E, and hysteresivity η, in the physiological range of airway smooth muscle stretch amplitudes and frequencies. The dashed lines, showing total F, E, and η, are the same as previously reported (Fredberg et al., 1999). At low strains ($\varepsilon < 1\%$) AM contributed significantly more to F and E compared to AMp. At higher stretch amplitudes, the sharp drop in AM compared to the modest decrease in AMp results in a decreased fractional contribution of AM to F; indeed, the myosin species that contributes most to mean force reverses between low- and high-stretch amplitudes. The fractional contributions of AM and AMp to the elastance, E, follow roughly the same pattern, but do not reverse. It can also be shown that the net elastance is, like the total force, a strictly additive function of the independent contributions of AM and AMp. Unlike the force and elastance, hysteresivity is the stiffness weighted change of its two components, and it is not additive. As expected from the time constants, we see that at $f =$ 0.33 Hz, hysteresivity of AM is small, whereas hysteresivity of AMp is substantial and grows with strain amplitude (see Fig. 7, *lower left panel*).

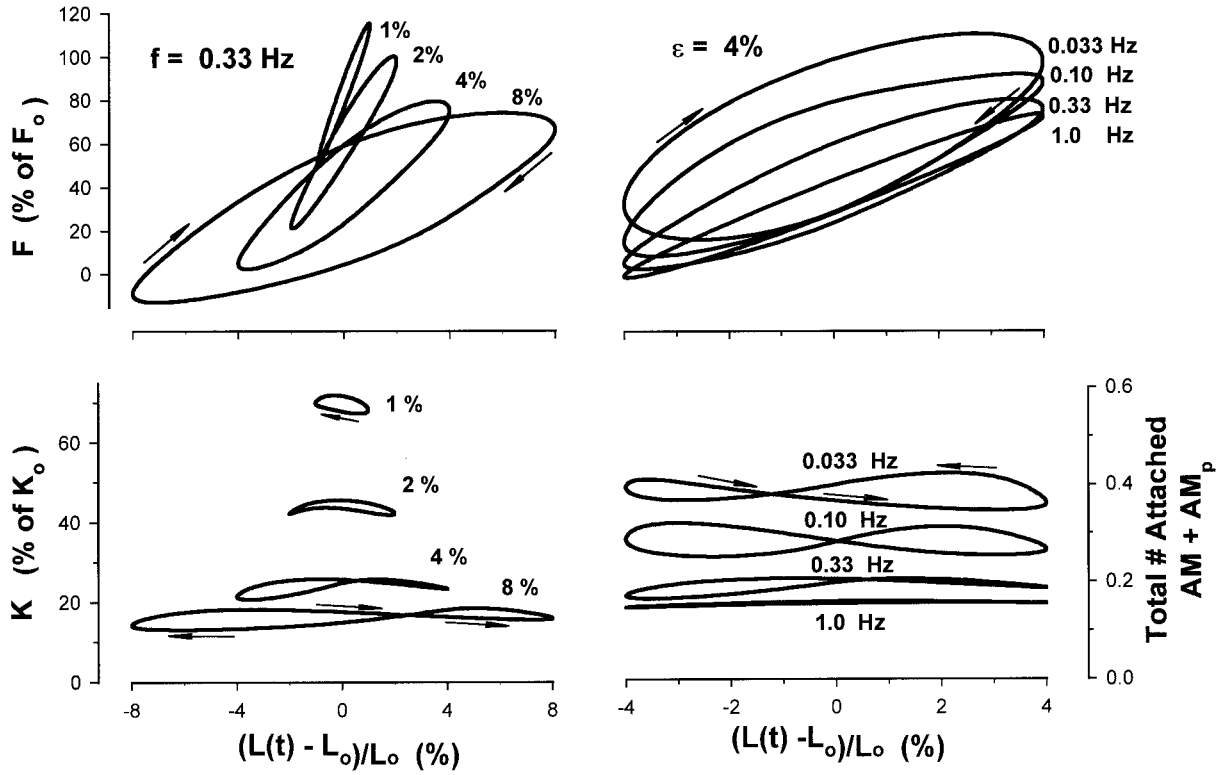

FIGURE 6 Instantaneous force–length and stiffness–length loops (of both AM and AMp bridges) for a family of strain amplitudes at the physiologic frequency of 0.33 Hz (*left panels*), and for a family of frequencies at 4% strain amplitude (*right panels*). Instantaneous force and stiffness are normalized to their isometric values.

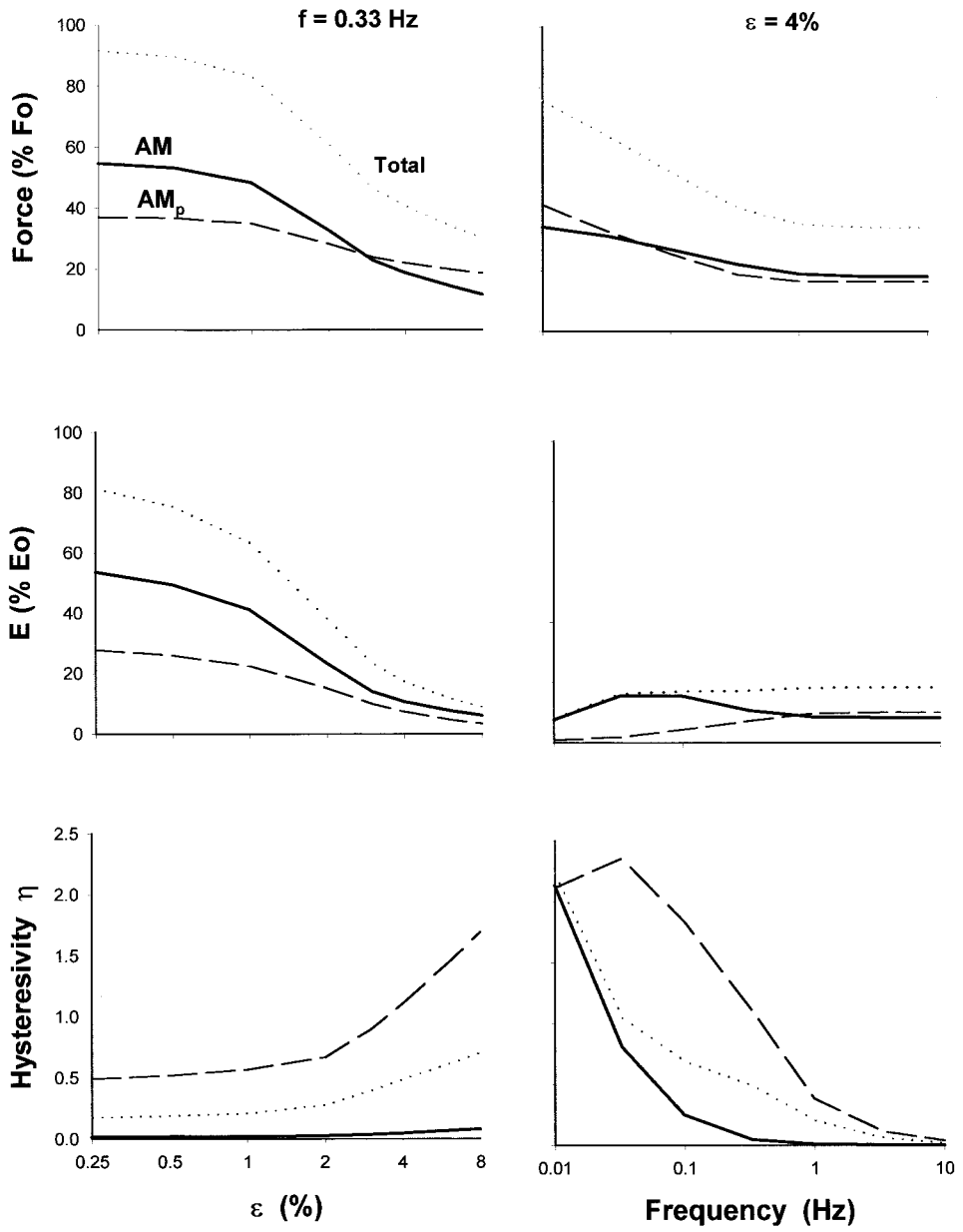

FIGURE 7 Total (*dotted line*) and fractional contributions of AM (*solid line*) and AMp (*dashed line*) to the mean force F, elastance E, and hysteresivity η as a function of strain amplitudes for a frequency of 0.33 Hz (*left panels*), and as a function of frequency for a strain amplitude of 4% (*right panels*). Mean force and stiffness are normalized to their isometric values.

The effect of frequency (at constant stretch amplitude of 4%) on F, E, and η is shown in Fig. 7, right panels. At this particular amplitude, the fractional contributions of AM and AMp to mean total F are about equal; all three decrease about twofold from low to middle frequencies (0.01–0.5 Hz), and then plateau for higher f. The fractional contributions of AM and AMp to overall E displayed a similar plateau at high frequencies. By contrast, in the low- to middle-frequency range, the contributions of AM and AMp to elastance are strikingly different. Specifically, as frequency decreases, the elastance is determined almost entirely by AM latch bridges.

Both AM and AMp display a sharp drop in hysteresivity with increasing frequency. This drop for the rapidly cycling AMp bridges occurs about one order of magnitude higher in frequency compared with the slower AM bridges. This is consistent with, and indeed a necessary consequence of, the fact that the rate constants for AMp bridges are about one order of magnitude larger than the AM bridges. This sharp increase in η and decrease in E with decreasing frequency is typical for a non-equilibrium phase transition (from solid-like or elastic-to-liquid-like or plastic behavior (Fredberg et al., 1999; De Gennes, 1979).

It is very interesting to note that in the low frequency range, the contributions of AMp and AM to E and η are sharply different, as expected from their different rate constants, but that their contributions to total mean force F remain roughly comparable. The origin of this is in the

independent effects of time-average cross-bridge strain and the variation of these strains over the cycle, which are different for AMp and AM cross-bridges. In particular, at low frequencies, the rapid cycling rates of AMp bridges promote attachment and, on average, only modestly varying mean strain over the cycle. Because AMp bridges quickly adapt, keeping most of the cross-bridges attached in the region ($0 < x < h$), they function essentially as constant force generators, with low elastance. By contrast, the slower AM bridges cannot adapt as quickly to the imposed length changes, and because of their slow detachment rate, their mean strain varies significantly over the loop more or less proportionally with imposed length variation. They are more elastic with high elastance and low hysteresivity.

Myosin duty cycle and energy cost of myosin binding

Myosin duty cycle

We define the myosin duty cycle to be the fraction of time that an average myosin head is attached to actin during steady-state length oscillations. This is equivalent to the time average of the fraction of attached bridges and is proportional to the time-average instantaneous muscle stiffness. At fixed frequency the duty cycle or average fraction of attached cross-bridges roughly parallels the behavior of both elastance and mean force as functions of strain amplitude, whereas at fixed strain amplitude, the duty cycle parallels the behavior of mean force, but not elastance as functions of frequency (Fig. 8 *A*). Thus, the duty cycle is rather more closely associated with mean force and average instantaneous stiffness than with elastance. The reason for this dissociation at low frequencies is that AMp bridges have enough time to adapt to a new length (and with further decrease in frequencies, also AM bridges), keeping most of the cross-bridges attached in the region ($0 < x < h$), increasing duty cycle (also maintaining high mean force and stiffness), in contrast to almost zero chord slope of AMp's force-length loops (for frequencies <0.033 Hz), that significantly decrease overall elastance.

Cycling rates and energy consumption

The ATPase activity computed from the net rate of bridge cycling (exclusive of phosphorylation events) is shown as ATP_{cycl}, and this quantity, together with the additional ATP

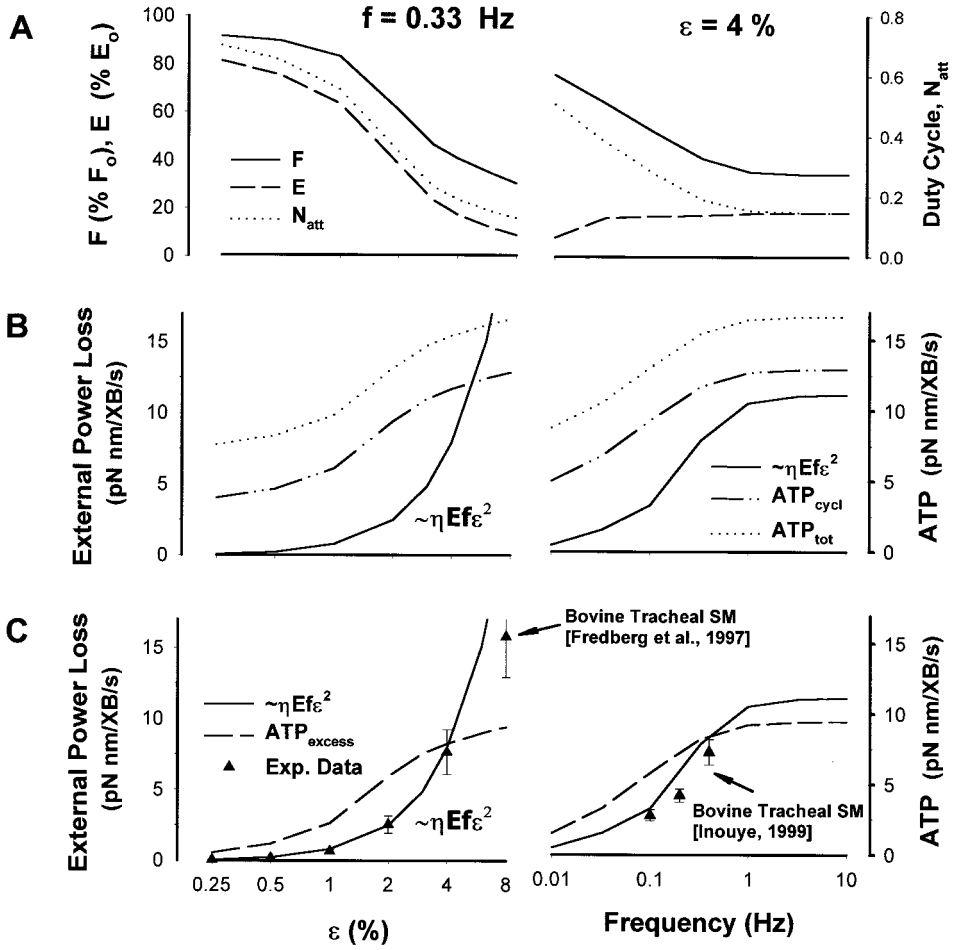

FIGURE 8 For the same range of stretch amplitudes and frequencies as in Fig. 7, this figure shows (*A*) duty cycle or average fraction of attached cross-bridges (*dotted line*), mean force (*solid line*), and elastance (*dashed line*) within airway smooth muscle. (*B*) Rate of external energy loss (power, *solid line*) and time average of ATPase. Also shown are ATP_{tot} (*dotted line*), and ATP_{cycl} (*dash-dot-dot line*). Note that $ATP_{tot} = ATP_{cycl} + ATP_{phosp}$, where ATP_{phosp} is steady-state ATPase of latch bridge maintenance. (*C*) Rate of external energy loss (HHM prediction, *solid line*), and that experimental points (from Fredberg et al. (1997) and Inouye (1999); *triangles* ±SD). Also shown is ATP_{excess} (*dashed line*), where $ATP_{excess} = ATP_{cycl} - ATP_{iso}$ is the excess ATPase activity over ATP_{iso}, the isometric steady-state cross-bridge ATPase. Both power energy loss and ATPase activity are calculated per a myosin molecule (XB). The free energy of ATP hydrolysis is assumed to be 100 pNnm.

consumption associated with phosphorylation events, defines the total, shown as ATP_{tot} (Fig. 8 *B*). The mechanical work done by the imposed strains on the muscle per cycle is equal to the area enclosed by the force/length loop *D*; the power loss is given by the average work done on the muscle per unit time, or in terms of our previously defined quantities, by $Df = \eta E \Delta L^2 f \pi$. Note first that the ATP consumption associated with phosphorylation events (i.e., ATP_{tot}–ATP_{cycl}) is independent of strain amplitude or frequency. Second, the mechanical power loss increases much more sharply than ATPase activity as a function of strain amplitude for fixed frequency, whereas the behaviors of the power loss and ATPase are quite similar as a function of frequency for fixed strain amplitude. It is important to note that both chemical energy of ATPase and the mechanical power loss are energy-dissipative processes.

The stretch-induced augmentation of the hysteresivity is attributable in part to a direct mechanical effect at the level of cyclic interaction of myosin and actin (Huxley, 1957; Eisenberg and Hill, 1985). Compared with isometric conditions, during tidal stretch the attached myosin molecule spends some fraction of each period in regions along the actin filament that favor rapid detachment ($x < 0$ and/or $h < x$). The greater the stretch amplitude, the greater would be that fraction. Dashed lines in Fig. 8 *C* show excess ATPase (over the isometric) that is caused by tidal stretches ($ATP_{excess} = ATP_{cycl} - ATP_{iso}$). Increased time spent in regions favoring detachment would, in turn, account for an increased rate of bridge turnover and an elevated value of η.

At small strains ($\varepsilon < 0.25\%$), ATP_{cycl} utilization is almost entirely spent on isometric force maintenance, while dissipated mechanical energy ($\sim \eta E f \varepsilon^2$) is small. At large strains ($\varepsilon > 4\%$) and $f \sim 0.33$ Hz, ATP_{cycl} increased three times in order to maintain the steady state, while dissipated rate of energy imposed on muscle increased much more with strain, exceeding not only ATP_{excess}, but also ATP_{cycl}. However, this excessive increase of η at stretches above 4% is not supported by previously reported experimental data shown in Fig. 10 *A* (from Fredberg et al., 1997, 1999), where η slightly decreases. Harry et al., 1990, also reported experimental disagreement with Huxley-type simulations of skeletal muscle lengthening. These discrepancies are most likely associated with departures of the rate functions for $|x| > h$, from those assumed in the simple model. We conclude that the HHM model is accurate for perturbations smaller than 4% of muscle length, but will need modification at larger amplitudes.

In order to investigate the above uncertainty of the HHM model rate constants at stretches above 4%, we also calculated power loss from the data shown in Fig. 10 *A* (from Fredberg et al., 1997, 1999); this is shown in Fig. 8 *C* (*triangles*). It agrees well with HHM predictions up to $\varepsilon = 4\%$. At $\varepsilon = 8\%$, however, we note two features. First, external power loss computed by HHM theory significantly overestimates the experimentally determined power loss. Second, the experimentally determined power loss is itself significantly higher than the HHM-computed ATPase activity. These two observations imply only a weak coupling between external mechanical work (power) and the chemical energy (cyclic ATPase) required for maintaining steady-state contraction.

A comparison of the ATPase behavior (Fig. 8, *B* and *C*) and the mean force and stiffness (or fraction attached) behavior (Fig. 8 *A*) as functions of both strain amplitude and frequency shows that the depression of force and stiffness associated with strain amplitude and frequency is accompanied by increased ATPase activity. In other words, the perturbed equilibrium requires external work to break the cross-bridges, which in turn raises the myosin cycling rates and therefore the biochemical energy required to maintain that dynamic equilibrium.

Hysteresivity and cross-bridge cycling rates

We have suggested previously that η is a reasonable index of cross-bridge cycling rates (Fredberg et al., 1996, 1997), although Shen et al. (1997) have disputed that assertion. Fig. 8 *C* shows that an increase in cycling rate (or ATP_{excess}, *dashed line*) is closely associated with external power loss (*solid line*), for strains up to ~3%. Beyond that point, however, power loss increases even more sharply with increasing strain, whereas ATP_{excess} tends to plateau. We conclude that η is a good index of cross-bridge cycling rates for small amplitudes, but departs at large strains, such as the 6% strain used by Shen et al. (1997). This observation reconciles Shen's finding with our previous reports.

We confirmed these ideas by examining the direct correlation between η and cross-bridge cycling rates (i.e., loop average of ATP_{cycl}), by varying the level of myosin phosphorylation at fixed length fluctuations of 2% and frequency of 0.33 Hz (Fig. 9). We found an approximately linear relationship between η and cross-bridge cycling rates. It is interesting to notice that η approaches a positive value of ~0.11 in the limit as myosin phosphorylation approaches zero, while the cross-bridge cycling rate approaches 0. To better understand this behavior at very low levels of phosphorylation, we investigated the relationship between ηE and ATP_{cycl} (also shown in Fig. 9). The HHM model predicts an almost linear relationship between ηE and ATP_{cycl}, consistent with the observations of Fredberg et al. (1996) in canine tracheal strips during force development. Note that during force development, phosphorylation levels in tracheal smooth muscle typically vary from almost zero to a maximum value of 0.65 mol Pi/mol LC_{20}, which spans a substantial portion of range of phosphorylation levels used in Fig. 9. Taken together, this analysis confirms a strong linear correlation between η and cross-bridge cycling rates, which is even stronger if ATP_{cycl} is normalized by number of attached cross-bridges, or equivalently, ηE is compared with ATP_{cycl} (as explicitly shown in Fig. 9).

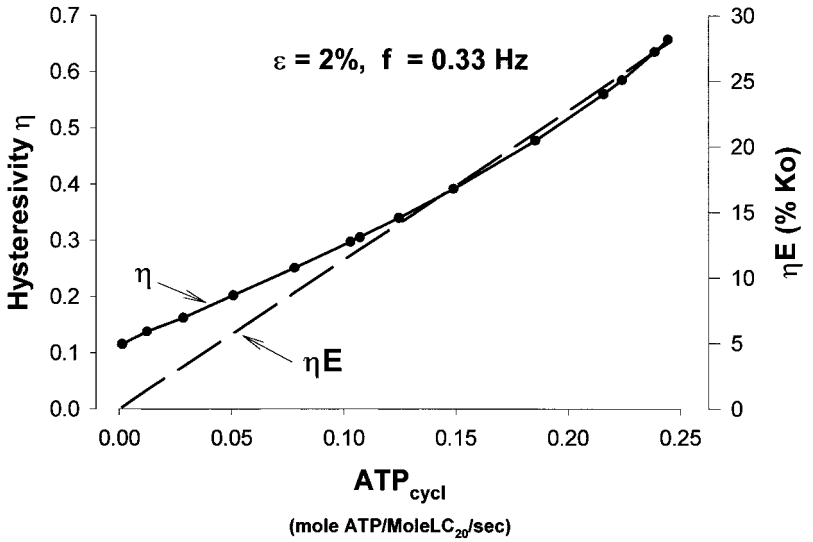

FIGURE 9 Hysteresivity, (η) on *left* *y*-axis (*solid line*) and loss modulus (ηE) (*dashed line*) as a function of ATP_{cycl} calculated different levels of phosphorylation (from 0.05 on the left to 0.99 at right). Amplitude of sinusoidal stretches was $\varepsilon = 0.25\%$ and frequency was 0.33 Hz. Loss modulus is normalized by isometric stiffness, K_0, at 100% of phosphorylation.

Is Huxley's two-state model sufficient to explain the effect of imposed cyclic tidal stretches?

Force depression with increasing strain amplitude, as shown in Fig. 7, is also observed in skeletal muscle (Rack and Westbury, 1974), which has been explained by the mechanism of Huxley's two-state model (Zahalak, 1986). In Fig. 10 the numerical solutions for the explicit HHM four-state latch regulatory scheme, integrated into Huxley's sliding filament model, are contrasted with experimental observations previously reported (Fredberg et al., 1997), and with the exact solutions for a two-state myosin binding scheme (J. P. Butler, Howard University, personal communication). The rate constants in the two-state scheme were derived directly from those in the four-state scheme after the method of Hai and Murphy (1988b), and are thought to represent the best two-state approximation of the explicit four-state scheme at the prescribed level of phosphorylation. Both theoretical schemes are seen to capture the essential features of the data for steady-state oscillatory conditions, but only for one particular level of (steady-state) phosphorylation (Fig. 10 *A*). This is expected because Huxley's original model is only a two-state analysis and, as such, cannot directly address the questions of multiple myosin binding states, partitioning of attached myosin between phosphorylated (rapidly cycling), and unphosphorylated (slowly cycling) species in smooth muscle (Hai and Murphy, 1988a), or the stretch-induced changes of that partitioning (Fredberg et al., 1999; Fredberg et al., in preparation). To investigate this further, the predictions of the HHM and two-state approximation model (with adjusted rate constants for particular steady-state levels of myosin phosphorylation by using the method of Hai and Murphy, 1988b) were compared for different levels of myosin phosphorylation (Fig. 10 *B*). Both models predict a similar increase of mean force and elastance (similar to Murphy (1994) in isometric preparation, but somewhat depressed by cycling stretches), and η increases almost linearly. The two-state approximation model consistently overestimated both mean force and E at lower levels of myosin phosphorylation. Both models show that coupling between Hai and Murphy's four-state scheme (1988a) and Huxley's strain-dependent rate constants is essential to describe the transient phosphorylation state (i.e., a continuously variable cross-bridge cycling rate). The important strength of the four-state model that is absent in any two-state approximation is the ability to capture the dynamic features of varying levels of myosin phosphorylation through its effect on bridge populations and ATP consumption. Furthermore, the four myosin states are necessary to account for the experimentally observed depression of quick-release velocity-force curves generated at longer times during isometric force development (Mijailovich et al., 1998). Moreover, the two-state approximation (of the four-state) model is not sufficient to accurately account for the time course of the isotonic shortening velocity after quick release because the internal resistance of the attached cross-bridges also depends on distributions of attached cross-bridges that can only be accounted for by the HHM model.

Implications in bronchospasm

Experiments and HHM theory, taken together, suggest that fluctuating mechanical strains imposed on the muscle are transmitted to the myosin head and cause it to detach from the actin filament much sooner than it would have in isometric circumstances. This premature detachment profoundly reduces the duty cycle of myosin. In the case of airway smooth muscle subjected to the load fluctuations associated with breathing, the duty cycle is typically reduced to ~20% of its value in the unperturbed isometric

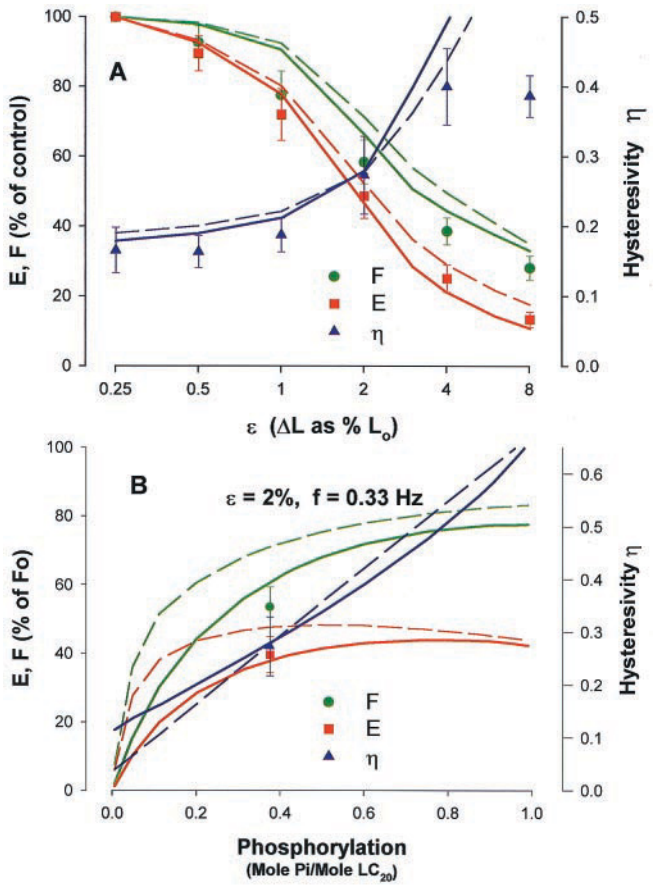

FIGURE 10 (*A*) Steady-state mean force, elastance, and hysteresivity as a function of strain amplitude at a steady-state level of phosphorylation of 0.375 mol Pi/mol LC_{20}. Experimental data from maximally activated tracheal smooth muscle (from Fredberg et al. (1997) normalized to 100% at $\varepsilon = 0.25\%$, frequency 0.33 Hz) are shown by closed symbols ±SD. The predictions of HHM theory are shown in the solid lines, and the predictions of the two-state Huxley (1957) model are shown in dashed lines. (*B*) Steady-state mean force, elastance, and hysteresivity as a function of myosin light chain phosphorylation at fixed frequency of 0.33 Hz and fixed amplitude of $\varepsilon = 2\%$. Mean force, *F*, and elastance, *E*, are normalized by the respective isometric values at 100% phosphorylation.

steady state, and total numbers of bridges attached and active force are depressed to a similar extent. Of the full isometric force generating capacity of the muscle, therefore, only a small fraction ever comes to bear to narrow the airway. In asthma, however, it is believed that the load fluctuations acting on myosin somehow become compromised—perhaps due to inflammatory remodeling of the airway wall. With dynamic unloading this potent inhibition is removed and the muscle then generates the full complement of isometric steady-state force appropriate to the stimulus. As a result, the airway can narrow to the point of closure. This may explain why airway narrowing is limited in the healthy lung but not in the asthmatic lung.

Several other mechanisms have been considered to explain the effects of tidal stretch on airway smooth muscle mechanics; these include stretch-activated neural pathways, stretch-activated prostanoid release, stretch-induced remodeling of the cytoskeleton, length-dependent changes in Ca^{2+} sensitivity, length-dependent myosin phosphorylation, and direct mechanical effects of stretch on bridge dynamics (Pratusevich et al., 1995; Sasaki and Hoppin, 1979; Fredberg et al., 1999; Gunst et al., 1995; Mehta et al., 1996; Hai, 1991). Although all these factors may be important, a system as superficially simple as Huxley's two-state sliding filament model embodies the essential changes of force, stiffness, and hysteresivity that occur acutely with the onset of sinusoidal stretch (Fig. 9). Therefore, features of Huxley's sliding filament model point to the dominant underlying mechanism of these stretch-induced changes; namely, disruption of the spatial distribution of myosin binding along the actin filament and the sustained departure of that bond distribution from the equilibrium distribution that pertains in the isometric steady state (compare perturbed HHM bond distributions in Fig. 4 and isometric steady state in Fig. 2 *D*).

On the basis of these results, it seems reasonable to conclude that the dynamically determined contractile states that have been reported previously in airway smooth muscle (Fredberg et al., 1997) are attributable in large part to the direct effects of tidal stretch on bridge dynamics. Perturbed equilibrium of myosin binding may have applicability in a variety of smooth muscle systems that are routinely subjected to tidal loading, but seems to explain in particular why tidal stretch of airway smooth muscle is such a potent endogenous relaxing mechanism.

NOTES

1. The force-displacements loops are closed only in oscillatory steady state. However, during force development and the transients during mean force adaptation to a different level of stretch amplitude, the instantaneous forces at the beginning and at the end of a cycle are somewhat different. Assuming linear change of the force difference over time, the open loops are closed by removing this trend and preserving the loop mean force.
2. The factor of 2 arises from the most parsimonious method of preserving the spatial mean attachment and detachment fluxes (given by the product of the respective rate functions and bond distributions). It is exact when the bond distribution is uniform. During force development the bond distributions are not uniform; the ratio of mean flux to the product of mean rate function and mean bond distribution departs from a constant and would correspond to this factor ranging from 1.5 to 2.75 (see also Yu et al., 1997). However, the force during force development is not too sensitive to this effect; it differs from Hai and Murphy's (1988a) results by $<3\%$.
3. Cross-bridge displacement of magnitude *h* corresponds to a whole muscle strain of $\sim\varepsilon = 4\%$ if cross-bridge strain is taken to be 36% of overall strain in order to account for the serial elastic component (Mijailovich et al., 1996). If we also assume that muscle stretch scales isotropically as the cube root of lung volume change (Hughes et al., 1972), then normal tidal lung inflation from FRC would correspond roughly to $\varepsilon = 4\%$, a sigh from FRC would correspond to $\varepsilon = 12\%$, and inflation from FRC to total lung capacity would correspond roughly to $\varepsilon = 25\%$ (Fredberg et al., 1997).

This work was supported by National Institutes of Health Grants HL 33009 and HL 59682.

REFERENCES

Altman, L., and D. S. Dittmer. 1974. Biology Data Book, Vol. III. FASEB, Bethesda, MD.

De Gennes, P. 1979. Scaling Concepts of Polymer Physics. Cornell University Press, Ithaca, NY.

Eisenberg, E., and T. L. Hill. 1985. Muscle contraction and free energy transduction in biological systems. *Science.* 227:999–1006.

Fredberg, J. J., D. Inouye, B. Miller, M. Nathan, S. Jafari, S. H. Raboudi, J. P. Butler, and S. A. Shore. 1997. Airway smooth muscle, tidal stretches, and dynamically determined contractile states. *Am. J. Respir. Crit. Care Med.* 156:1752–1759.

Fredberg, J. J., K. A. Jones, M. Nathan, S. Raboudi, Y. S. Prakash, S. A. Shore, J. P. Butler, and G. C. Sieck. 1996. Friction in airway smooth muscle: mechanism, latch and implications in asthma. *J. Appl. Physiol.* 81:2703–2712.

Fredberg, J. J., S. M. Mijailovich, and J. P. Butler. 1999. Perturbed equilibrium of myosin binding in airway smooth muscle and its implications on bronchospasm. *Am. J. Respir. Crit. Care Med.* 159:959–967.

Fredberg, J. J., and D. Stamenovic. 1989. On the imperfect elasticity of lung tissue. *J. Appl. Physiol.* 67:2408–2419.

Gunst, S. J., R. A. Meiss, M.-F. Wu, and M. Rowe. 1995. Mechanisms for the mechanical plasticity of tracheal smooth muscle. *Am. J. Physiol. Cell Physiol.* 268:C1267–C1276.

Gunst, S. J., J. Q. Stropp, and J. Service. 1990. Mechanical modulation of pressure-volume characteristics of contracted canine airways in vitro. *J. Appl. Physiol.* 68:2223–2229.

Hai, C. M. 1991. Length-dependent myosin phosphorylation and contraction of arterial smooth muscle. *Pflugers Arch.* 418:564–571.

Hai, C. M., and R. A. Murphy. 1988a. Cross-bridge phosphorylation and regulation of latch state in smooth muscle. *Am. J. Physiol. Cell Physiol.* 254:C99–C106.

Hai, C. M., and R. A. Murphy. 1988b. Regulation of shortening velocity by cross-bridge phosphorylation in smooth muscle. *Am. J. Physiol. Cell Physiol.* 255:C86–C94.

Harry, J. D., A. W. Ward, N. C. Heglund, D. L. Morgan, and T. A. McMahon. 1990. Cross-bridge cycling theories cannot explain high-speed lengthening behavior in frog muscle. *Biophys. J.* 57:201–208.

Hughes, J. M. B., F. G. Hoppin, Jr., and J. Mead. 1972. Effect of lung inflation on bronchial length and diameter in excised lungs. *J. Appl. Physiol.* 32:25–35.

Huxley, A. F. 1957. Muscle structure and theories of contraction. *Prog. Biophys. Biophys. Chem.* 7:255–318.

Inouye, D. 1999. The perturbed equilibrium of myosin binding in airway smooth muscle and its implications in airway hyperresponsiveness and asthma. Ph.D. thesis, MIT, Cambridge, MA.

Klemt, P., U. Peiper, R. N. Speden, and F. Zilker. 1981. The kinetics of post-vibration tension recovery of the isolated rat portal vein. *J. Physiol.* 312:281–296.

Mehta, D., M.-F. Wu, and S. J. Gunst. 1996. Role of contractile protein activation in the length-dependent modulation of tracheal smooth muscle force. *Am. J. Physiol. Cell Physiol.* 270:C243–C252.

Mijailovich, S. M., J. J. Fredberg, and J. P. Butler. 1996. On the theory of muscle contraction: filament extensibility and the development of isometric force and stiffness. *Biophys. J.* 71:1475–1484.

Mijailovich, S. M., J. J. Fredberg, and J. P. Butler. 1998. Implications of the latch model of smooth muscle contraction: shortening velocity and bridge dynamic during quick release. *Biophys. J.* 74:156*a* (Abstr.)

Murphy, R. A. 1994. What is special about smooth muscle? The significance of covalent crossbridge regulation. *FASEB J.* 8:311–318.

Peiper, U., S. C. Knip, B. Thies, and R. Henke. 1996. Activation of protein kinase C accelerates contraction kinetics of airway smooth muscle. *Pflügers Arch.* 432:R47–R52.

Piazzesi, G., and V. Lombardi. 1995. A cross-bridge model that is able to explain mechanical and energetic properties of shortening muscle. *Biophys. J.* 68:1966–1979.

Pratusevich, V. R., C. Y. Seow, and L. E. Ford. 1995. Plasticity in canine airway smooth muscle. *J. Gen. Physiol.* 105:73–94.

Rack, P. M., and D. R. Westbury. 1974. The short range stiffness of active mammalian muscle and its effect on mechanical properties. *J. Physiol.* 240:331–350.

Sasaki, H., and F. G. Hoppin, Jr. 1979. Hysteresis of contracted airway smooth muscle. *J. Appl. Physiol.: Respirat. Environ. Exercise Physiol.* 47:1251–1262.

Seow, C. Y., and N. L. Stephens. 1987. Time dependence of series elasticity in tracheal smooth muscle. *J. Appl. Physiol.* 62:1556–1561.

Shen, X., M. F. Wu, R. S. Tepper, and S. J. Gunst. 1997. Pharmacological modulation of the mechanical response of airway smooth muscle to length oscillation. *J. Appl. Physiol.* 83:739–745.

Warner, D. O., and S. J. Gunst. 1992. Limitation of maximal bronchoconstriction in living dogs. *Am. Rev. Respir. Dis.* 145:553–560.

Yu, S., P. E. Crago, and H. J. Chiel. 1997. A nonisometric kinetic model for smooth muscle. *Am. J. Physiol. Cell Physiol.* 272:C1025–C1039.

Zahalak, G. I. 1986. A comparison of the mechanical behavior of the cat soleus muscle with a distribution-moment model. *J. Biomech. Eng.* 108:131–140.